Lattice strain and lattice expansion of the $SrRuO_3$ layers in $SrRuO_3/PbZr_{0.52}Ti_{0.48}O_3/SrRuO_3$ multilayer thin films

C. L. Jia,[a] J. Rodríguez Contreras, U. Poppe, H. Kohlstedt, R. Waser, and K. Urban
Institut für Festkörperforschung, Forschungszentrum Jülich GmbH, D-52425 Jülich, Germany

(Received 4 February 2002; accepted for publication 11 April 2002)

In $SrRuO_3/PbZr_{0.52}Ti_{0.48}O_3/SrRuO_3$ multilayer thin films on $SrTiO_3$ substrates the different lattice distortion behavior of the top and the bottom $SrRuO_3$ film layer is found and characterized by means of transmission electron microscopy. The bottom $SrRuO_3$ layer is compressively strained in the film plane by a constraint of the $SrTiO_3$ substrate. In contrast, in the interface area of the top $SrRuO_3$ layer, a lattice dilatation is measured not only in the film plane but also parallel to the film normal. The misfit strain, the lead interdiffusion and the oxygen concentration in this area are investigated and discussed as possible reasons for the unexpected lattice dilatation along the film normal direction. © *2002 American Institute of Physics.* [DOI: 10.1063/1.1483369]

I. INTRODUCTION

Electroceramic thin film systems are currently under intensive investigation for applications in advanced microelectronics.[1] Intensive research efforts are dedicated to studying and understanding deviations from the bulk material properties observed in epitactic systems resulting from lattice mismatch strain and lattice defects.[2] For example, a compressive epitaxial strain in thin films of $La_{2-x}Sr_xCuO_4$ has been found to increase this material's superconducting transition temperature.[3] The strain level in the film systems can be controlled by employing suitable buffer layers between substrate and film. For instance, in the $La_2CuO_4/LaSrAlO_4/SrTiO_3$ system the stain level and thus the superconducting properties of the La_2CuO_4 films were found to depend on the thickness of the $LaSrAlO_4$ buffer layer.[4,5] A large effect on the dielectric properties of $Ba_{0.6}Sr_{0.4}TiO_3$ films on MgO (001) substrates was observed when very thin strain layers of $Ba_{1-x}Sr_xTiO_3$ ($0.1 \leqslant x \leqslant 0.7$) were employed as buffers.[6]

$SrRuO_3$, one of the metallically conducting perovskites, is not only a promising candidate for electrode materials in electroceramic-based devices,[7–10] it also plays an important role in buffer technology for improving the quality of the device layer in multilayer systems. For example, high quality $SrTiO_3$ films with near single-crystal level dielectric losses have been obtained using a $SrRuO_3$ buffer on $LaAlO_3$ substrate.[11] The microstructure and defect configuration of this buffer layer were found to play an important role in the quality of the $SrTiO_3$ film.[12] $SrRuO_3$ has an orthorhombic structure with $a = 0.5567$ nm, $b = 0.553\,04$ nm and $c = 0.784\,46$ nm.[13] However, for many simple geometric considerations it is sufficient to refer to a pseudocubic cell with a cell parameter of 0.3923 nm. This parameter is very similar to the lattice parameter of 0.3905 nm of $SrTiO_3$.

In this article we report on the structural investigation by means of transmission electron microscopy (TEM) and high-resolution transmission electron microscopy (HRTEM) of the $SrRuO_3$ layers serving as electrodes in $SrRuO_3/Pb(ZrTi)O_3/SrRuO_3$ multilayer tunnel junctions on $SrTiO_3$ substrates.[14,15] The main interest is focused on the epitaxial strain in different film layers and lattice imperfections occurring in the interface areas.

II. EXPERIMENT

The samples used in the present work are $SrRuO_3/PbZr_{0.52}Ti_{0.48}O_3/SrRuO_3$ triple-layer films with two different sets of layer thicknesses, 36 nm/4 nm/15 nm (type 1) and 100 nm/10 nm/40 nm (type 2). They were deposited on $SrTiO_3$ substrates using high-pressure on-axis sputtering.[16] The substrate temperature and oxygen pressure used for the growth of both $SrRuO_3$ and $PbZr_{0.52}Ti_{0.48}O_3$ layers were about 580 °C and 3 mbar, respectively. The stoichiometry of the individual layers was verified by Rutherford backscattering spectrometry.[15] According to the pseudocubic lattice parameter of $SrRuO_3$ [in the following abbreviated as (SRO)] the lattice parameter is 0.5% larger than that of $SrTiO_3$ (STO). Compared to $PbZr_{0.52}Ti_{0.48}O_3$ (PZT) the lattice parameter is 2.7% smaller in the *a*-*b* plane and 5% smaller along the *c*-axis parallel to the film sequence.

Cross-sectional samples were prepared for TEM and HRTEM investigations. Slices of 2×1 mm^2 in size were cut from the film-covered wafers along the (100) plane of the STO substrate. Two of the slices were glued face to face and then embedded in epoxy resin. After the glue had been cured disks of 3 mm in diameter were obtained by cutting away redundant epoxy. These disks were then mechanically ground, dimpled, and polished from both sides until the thickness of the central area was less than 10 μm. The final thinning was performed by means of ion milling on a sample stage cooled by liquid nitrogen. The TEM and HRTEM investigations were carried out on a JEOL 4000EX electron microscope operated at 400 kV.

III. RESULTS

Figure 1 shows a cross-sectional high-resolution electron microscopic image of the type 1 film system. This lattice-

[a]Electronic mail: c.jia@fz-juelich.de

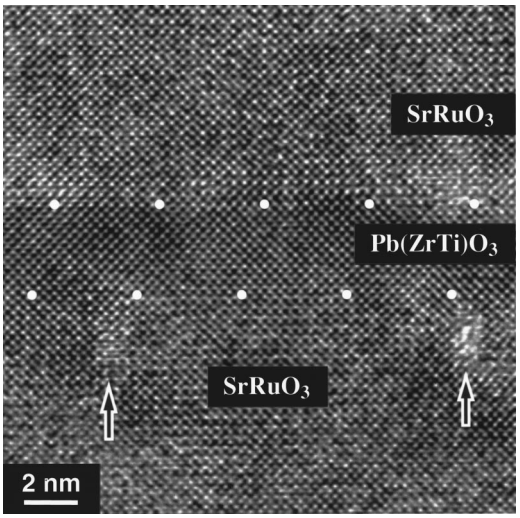

FIG. 1. Cross-sectional [100] lattice image of the $SrRuO_3/PbZr_{0.52}Ti_{0.48}O_3/SrRuO_3$ triple layer film with a 4 nm $PbZr_{0.52}Ti_{0.48}O_3$ barrier layer. The arrows denote misfit dislocations which are located at the lower interface area.

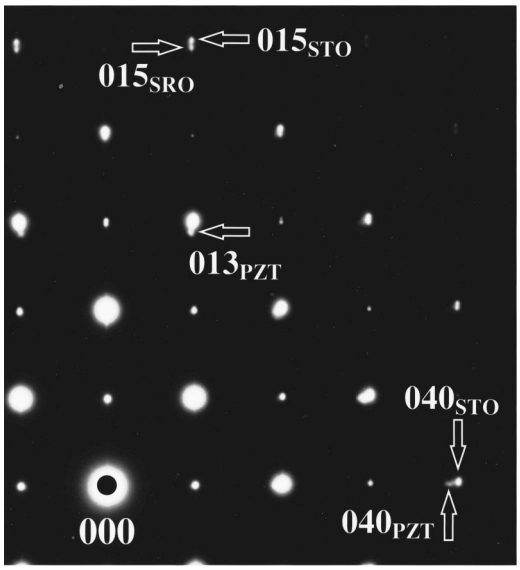

FIG. 2. Superposed electron diffraction pattern including the crystallographic information of all the film layers, $SrRuO_3$ (SRO), $PbZr_{0.52}Ti_{0.48}O_3$ (PZT), and the $SrTiO_3$ (STO) substrate.

fringe image was recorded with the electron beam parallel to a ⟨100⟩ direction in the film plane. The interfaces between the PZT layer and the two SRO electrode layers are marked by dots. Two misfit dislocations are denoted by arrows in the interface area of the bottom electrode layer. At the interface area of the top SRO electrode no misfit dislocations are found. Qualitatively similar results were observed in the type 2 film system. For better statistics we systematically investigated a 200 nm wide area along the interface and observed 13 misfit dislocations with a Burgers vector of $a\langle 010\rangle$ (modulus: 0.4 nm) at the lower interface. In contrast, only one dislocation was found at the upper interface. Nevertheless, in the type 2 film systems dislocations also occur in the upper SRO layer, although starting from about 10 nm above the interface. Due to the cubic symmetry of the STO substrate, the microstructure of the films must be the same in both the [100] and the [010] in-plane directions. Therefore, in the two orthogonal directions the distribution of the misfit dislocations is expected to be the same.

We studied the lattice parameters of the individual film layers by means of an analysis of the respective electron diffraction patterns (EDPs). Figure 2 shows an EDP of the type 2 film system recorded with the electron beam parallel to a ⟨100⟩ zone axis of the STO substrate. This EDP contains the crystallographic information of all the film layers and the substrate since it was recorded using a selected area aperture covering the whole trilayer film and, in addition, part of the substrate. From the pattern the reflection spots of the individual layers and of the substrate can be identified and partially indexed using the notation of the perovskite pseudocubic basic cells. In the following discussion, we denote the *c*-axis direction as parallel to the normal of the film plane (the growth direction of the film) and the *a* and *b* axis as lying in the plane. The difference in the *c*-lattice parameter between the three types of compounds can be clearly seen from the occurrence of the double $\{00l\}$ reflection spots along the vertical direction. The relaxation of the in-plane misfit strain in the PZT layer is also visible from the split of the (040) reflection spots of PZT and STO in the horizontal direction. No lattice relaxation in the electrode SRO layer with respect to the STO substrate can be recognized since there is no horizontal shift of the reflections detectable even for the high-index spots. The lattice behavior of the bottom electrode layer can be isolated from the top layer using a selected area diffraction aperture covering part of the bottom electrode layer and the substrate only. However, the lattice parameter of the top electrode layer cannot be precisely determined. The reason for this is that in the EDP the information on the top layer is not easy to distinguish unambiguously from that of the bottom layer due to the low accuracy of the location of the aperture. The other problem is the lack of a calibration standard. The superposed EDP of the STO substrate and the top SRO layer is impossible to isolate from that of the bottom SRO and the PZT layers which are sandwiched between them.

Taking the reflections and the bulk lattice parameter of STO as a calibration standard the results calculated for the bottom SRO and the PZT layers are listed in Table I. In the investigated films no difference was detected between *a* and *b* for the individual film layer. In comparison with the bulk parameters, the bottom SRO electrode layer is compressively strained in the film plane and its in-plane lattice parameter follows that of the substrate. Considering the lattice param-

TABLE I. Lattice parameters of the bottom SRO layer (100 nm) and the PZT layer (10 nm) calculated from the superposed electron diffraction patterns with reference to the reflection spots of STO. The notation of the lattice parameters is based on the perovskite basic unit cell.

Axis	*a* (nm)	*b* (nm)	*c* (nm)
STO	0.3905	0.3905	0.3905
SRO_B	0.3905	0.3905	0.3970
PZT	0.4040	0.4040	0.4128

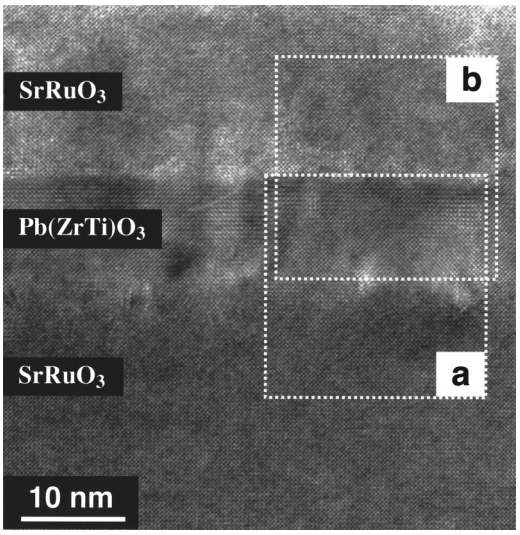

FIG. 3. [100] lattice image of the triple layer film with a 10 nm $PbZr_{0.52}Ti_{0.48}O_3$ layer. The frames a and b mark the areas for Fourier transformation.

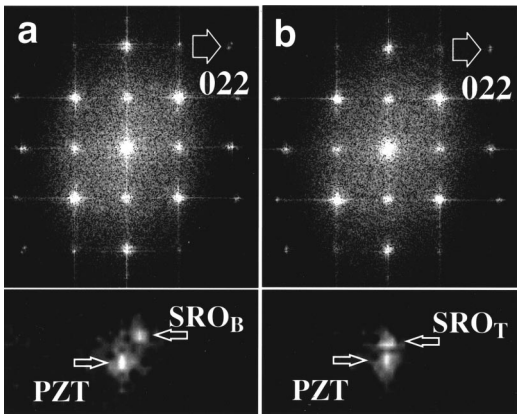

FIG. 4. Power spectra from areas a, PZT+bottom SRO layer (SRO_B) and b, PZT+top SRO layer (SRO_T). The spectrum spots denoted by the thick arrows are magnified and shown correspondingly below the spectra.

eter of the substrate, the bottom electrode layer is forced to adopt a tetragonal structure with the elongated *c*-axis parallel to the film normal. The loss of bulk symmetry (orthorhombic) could also be demonstrated by the EDP along the [110] zone axis of $SrTiO_3$. The PZT layer shows a lattice parameter very close to that of the bulk and the *c* axis is found to be parallel to the film normal.

We also investigated the lattice parameter of the interface areas on the basis of an analysis of the power spectrum of Fourier-transformed HREM lattice images. Of particular interest is the interface area of the upper SRO layer where the misfit dislocations are absent. As shown in Fig. 3, we chose the type 2 film system in order to obtain a strong signal of the PZT lattice, which was used as a standard in this procedure. Two frames in the image, denoted by a and b, respectively, mark two 20×20 nm areas including the same part of the PZT layer and a part of the bottom and a part of the top SRO layer. Two power spectra corresponding to the areas covered by the two frames were obtained by performing a numerical Fourier transform of the lattice images. As in the EDP, the position of the ''diffraction'' spots is inversely proportional to the local spacing of the lattice fringes appearing in the image. In order to obtain good statistics we obtained, by moving the two frames along the interface, a group of spectrum pairs for an *a* and a *b* area involving the same PZT layer area. Figure 4 shows an example of the Fourier spectrum pairs. Using the PZT spots as a reference we find that the bottom SRO layer area (SRO_B) shows a considerably different lattice fringe spacing compared to the top layer area (SRO_T). As demonstrated in the magnified part of the spectra denoted by arrows, in spectrum (a) the [022] spot of the bottom SRO layer exhibits both vertical and horizontal shift with respect to that of the PZT layer. However, the [022] spot of the top SRO layer area in spectrum (b) shows a vertical shift only. Taking the lattice parameter of the PZT layer obtained from EDP as the calibration standard, the lattice parameters of the bottom layer can be calculated. They show good agreement with those obtained from the EDP taken from SRO directly. This justifies the following measurements in Fig. 4. Based on the data of the PZT and the bottom SRO layers, the lattice parameters of the top SRO layer area were obtained as $a=0.3996$ nm and $c=0.3990$ nm. This means that we have a lattice expansion in both the *a* and the *c* direction of about 1.7% with respect to the bulk value.

The detailed variation of the *c*-lattice parameter with distance from the interface in the upper interface area was further investigated by lattice mapping directly on the image of the interface area using a numerical center-of-mass approach. Figure 5(a) shows an area of the upper interface rotated counterclockwise by 90° with respect to Fig. 3. In this image the left part is the top SRO layer area and the right part the PZT area. The crosses mark the mass center of the image dots corresponding to the cation columns viewed along the [100] direction of the pseudocubic structure. Figure 5(b) depicts a plot of *a*- and *c*-axis parameters of the two areas with the distance (number of unit cells) from the interface. According to the abrupt change in the *c* lattice parameters, the interface is geometrically very sharp and the relative values of this parameter for the two areas are very close to those obtained on the basis of the power spectra. There is no change of the *c*-lattice parameter with the distance up to 8 nm away from the interface. However, the a lattice parameter plot exhibits a slight decrease of the in-plane lattice parameter in the direction from the PZT layer to the SRO layer, reflecting the small difference in the in-plane lattice parameters.

IV. DISCUSSION

Our measurements clearly indicate a different behavior of the two SRO layers. The bottom layer exhibits the typical behavior under a compressive constraint of the substrate, that is a lattice expansion parallel to the film-plane normal accompanied by an in-plane compressive strain. In contrast, the interface area of the top SRO layer exhibits a lattice expansion in plane as well as along the plane normal. According to the general elasticity theory a lattice expansion in a plane should be accompanied by a shrinkage of the lattice dimen-

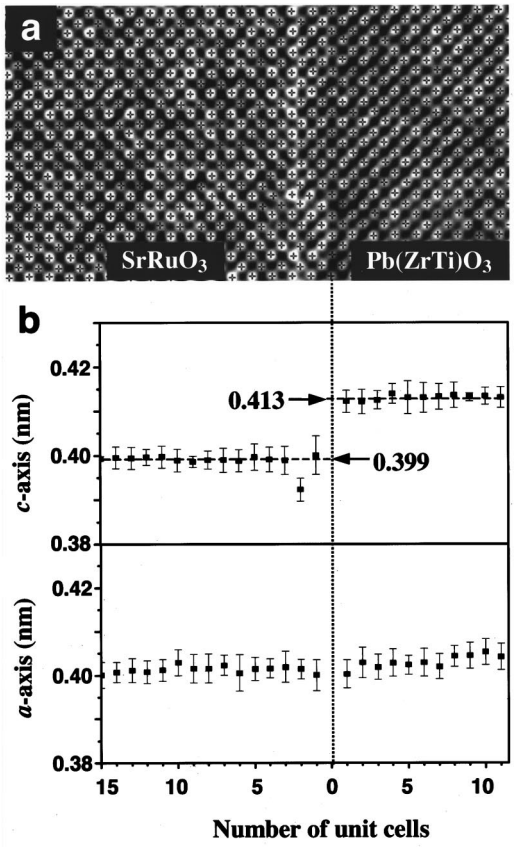

FIG. 5. (a) [100] image of the upper interface area. The crosses mark the mass center of the image dots corresponding to the cation columns; (b) plot of the *a*- and *c*-axis parameters with the distance from the interface plane.

sion perpendicular to the plane. Therefore, the lattice expansion measured here cannot be explained in terms of simple elastic misfit strain.

A possible explanation for our observation can be obtained taking into account the possibility of chemical interdiffusion across the interface during high-temperature film deposition. Lead does indeed form the equivalent compound $SrPbO_3$. Its pseudocubic lattice parameter of 0.417 nm is 6% larger than that of $SrRuO_3$ making the mixed $Sr(PbRu)O_3$ compound a good candidate for relaxation of the in-plane misfit strain at the interface to PZT. In addition it is well known that Pb can substitute for Ru in $SrRuO_3$. We used energy dispersive x-ray spectroscopy in the electron microscope to analyze the local composition in the interface area of the upper $SrRuO_3$ layer. Up to 3 at. % of Pb could be detected. However, we note that this amount is not sufficient to account for the measured lattice expansion. According to x-ray diffraction data a maximum lattice expansion of only 0.4% is expected for 3 at. % of Pb replacing Ru.[17]

A contribution of a possible deviation of the oxygen concentration from the stoichiometric value can also play a role. Both an excess and a deficiency of oxygen can in principle occur in the top layer areas, depending on the deposition conditions. The resulting deviation from stoichiometry can be accommodated by a variation of the valence of Ru cations. Considering the variable valence of Ru,[18–21] a change of the Ru ion valency from +4 to +3 does not only allow the oxygen vacancies to be accommodate but also leads to an increase of the ionic radius of Ru and thus to an expansion of lattice. In the case of strong oxidation conditions an excess of oxygen can also occur. This can be accompanied by a +5 valency of Ru. The excess oxygen may be accommodated in interstitial positions which, in turn, would lead to an expansion of the lattice. Although the same deposition conditions for both bottom and top SRO layers were used, the larger lattice mismatch between SRO and PZT than that between SRO and STO can heavily strain the lattice of the top SRO layer during growth. This lattice strain can contribute to the driving force for the concentration deviation of oxygen from the stoichiometry if the deviation can lower the strain energy. Nevertheless, it is still not clear how much of the lattice expansion can be accommodated by the concentration deviation of oxygen. From the effect of the Pb interdiffusion, it seems that the residual 1.3% expansion cannot only be due to the concentration deviation of oxygen. There may be other factors to contribute to the unsual lattice expansion.

On the other hand, we should also note the effect of the relaxation of the epitaxial strain due to the small thickness of the thin TEM specimen.[22] The lattice expansion along the viewing direction can be smaller than the measured velues from the lattice image.

V. CONCLUSIONS

We investigated the microstructure of tunnel junction multilayer films of $SrRuO_3/PbZr_{0.52}Ti_{0.48}O_3/SrRuO_3$ deposited on $SrTiO_3$ substrates. Taking the substrate data as calibration standard the lattice parameters of the three individual layers are measured evaluating electron diffraction patterns and high-resolution lattice images. The PZT barrier layer of both sample systems, type 1 (4 nm layer thickness) and type 2 (10 nm), show essentially the same structure and lattice parameter as the bulk material. However, the strain status and lattice parameter of the two SRO electrode layers are very different from each other. The bottom layer is under an in-plane constraint of the substrate lattice and shows a tetragonal structure with the long axis parallel to the film normal. The top layer exhibits a large lattice expansion both in the interface plane and perpendicular to it. This expansion can be understood in terms of interdiffusion of Pb substituting for Ru in the SRO lattice and in terms of a deviation of the oxygen concentration from stoichiometry. The increase of the Ru ion radius arising from the corresponding adjustment of the Ru valency can supply additional contributions to lattice expansion.

ACKNOWLEDGMENTS

The authors thank J. Schubert and N. A. Pertsev for discussions. This work was supported by the Volkswagen-Stiftung and in part by the HGF-Startegiefonds "Piccolo."

[1] N. Setter and R. Waser, Acta Mater. **48**, 151 (2000).
[2] A. G. Zembilgotov, N. A. Pertsev, H. Kohlstedt, and R. Waser, cond-mat/0111218.
[3] J.-P. Locquet, J. Perret, J. Fompeyrine, E. Mächler, J. W. Seo, and G. Van Tendeloo, Nature (London) **394**, 453 (1998).
[4] W. Si and X. X. Xi, Appl. Phys. Lett. **78**, 240 (2001).

[5] C. L. Jia, X. H. Zeng, X. X. Xi, and K. Urban, Phys. Rev. B **64**, 075416 (2001).
[6] B. H. Park, E. J. Peterson, Q. X. Jia, J. Lee, X. Zeng, W. Si, and X. X. Xi, Appl. Phys. Lett. **78**, 533 (2001).
[7] C. B. Eom, R. J. Cava, R. M. Fleming, J. M. Phillips, R. B. van Dover, J. H. Marshall, J. W. P. Hsu, J. J. Krajewski, and W. F. Peeck, Jr., Science **258**, 1776 (1993).
[8] C. B. Eom, R. B. van Dover, J. M. Phillips, D. J. Werder, J. H. Marshall, C. H. Chen, R. J. Cava, R. M. Fleming, and D. K. Fork, Appl. Phys. Lett. **63**, 2570 (1993).
[9] Q. X. Jia, S. R. Foltyn, M. Hawley, and X. D. Wu, J. Vac. Sci. Technol. A **15**, 1080 (1997).
[10] C. L. Chen, Y. Cao, Z. J. Huang, Q. D. Jiang, Z. Zhang, Y. Y. Sun, W. N. Kang, W. K. Chu, and C. W. Chu, Appl. Phys. Lett. **71**, 1047 (1997).
[11] H. C. Li, W. D. Si, A. D. West, and X. X. Xi, Appl. Phys. Lett. **73**, 190 (1998).
[12] J. S. Wu, C. L. Jia, K. Urban, J. H. Hao, and X. X. Xi, J. Appl. Phys. **89**, 5653 (2001); Philos. Mag. Lett. **81**, 375 (2001); J. Mater. Res. **16**, 3443 (2001).
[13] C. W. Jones, P. D. Battle, P. Lightfoot, and W. T. A. Harrison, Acta Crystallogr., Sect. C: Cryst. Struct. Commun. **45**, 365 (1989).
[14] H. Kohlstedt, J. Rodríguez Contreras, U. Poppe, C. L. Jia, R. Waser, J. Schubert, and N. A. Pertsev (unpublished).
[15] J. Rodríguez Contreras, J. Schubert, U. Poppe, K. Szot, C. L. Jia, H. Kohlstedt, and R. Waser, MRS Fall Meeting Boston, 2001 (to be published).
[16] U. Poppe, J. Schubert, R. R. Arons, W. Evers, C. H. Freiburg, W. Reichert, K. Schmidt, W. Sybertz, and K. Urban, Solid State Commun. **66**, 661 (1988).
[17] G. Cao, S. McCall, J. Bolivar, M. Shepard, F. Freibert, P. Henning, J. E. Crow, and T. Yuen, Phys. Rev. B **54**, 15144 (1996).
[18] H. Kobayashi, M. Nagata, R. Kanno, and Y. Kawamoto, Mater. Res. Bull. **29**, 1271 (1994).
[19] R. J. Bouchard and J. F. Weiher, J. Solid State Chem. **4**, 80 (1972).
[20] R. S. Liu, L.-Y. Jang, H.-H. Hung, and J. L. Tallon, Phys. Rev. B **63**, 212507/1 (2001).
[21] P. G. Clem, D. A. Payne, and W. L. Warren, J. Appl. Phys. **77**, 5865 (1995).
[22] M. M. J. Treacy, J. M. Gibson, and A. Howie, Philos. Mag. A **51**, 389 (1985).